

TransCom model simulations of methane: Comparison of vertical profiles with aircraft measurements

Ryu Saito,¹ Prabir K. Patra,^{1,2} Colm Sweeney,³ Toshinobu Machida,⁴ Maarten Krol,^{5,6} Sander Houweling,⁶ Philippe Bousquet,⁷ Anna Agusti-Panareda,⁸ Dmitry Belikov,⁴ Dan Bergmann,⁹ Huisheng Bian,¹⁰ Philip Cameron-Smith,⁹ Martyn P. Chipperfield,¹¹ Audrey Fortems-Cheiney,⁷ Annemarie Fraser,¹² Luciana V. Gatti,¹³ Emanuel Gloor,¹¹ Peter Hess,¹⁴ Stephan R. Kawa,¹⁰ Rachel M. Law,¹⁵ Robin Locatelli,⁷ Zoe Loh,¹⁵ Shamil Maksyutov,⁴ Lei Meng,¹⁶ John B. Miller,³ Paul I. Palmer,¹² Ronald G. Prinn,¹⁷ Matthew Rigby,^{17,18} and Christopher Wilson¹¹

Received 27 September 2012; revised 27 March 2013; accepted 28 March 2013; published 13 May 2013.

[1] To assess horizontal and vertical transports of methane (CH₄) concentrations at different heights within the troposphere, we analyzed simulations by 12 chemistry transport models (CTMs) that participated in the TransCom-CH₄ intercomparison experiment. Model results are compared with aircraft measurements at 13 sites in Amazon/Brazil, Mongolia, Pacific Ocean, Siberia/Russia, and United States during the period of 2001–2007. The simulations generally show good agreement with observations for seasonal cycles and vertical gradients. The correlation coefficients of the daily averaged model and observed CH₄ time series for the analyzed years are generally larger than 0.5, and the observed seasonal cycle amplitudes are simulated well at most sites, considering the between-model variances. However, larger deviations show up below 2 km for the model-observation differences in vertical profiles at some locations, e.g., at Santarem, Brazil, and in the upper troposphere, e.g., at Surgut, Russia. Vertical gradients and concentrations are underestimated at Southern Great Planes, United States, and Santarem and overestimated at Surgut. Systematic overestimation and underestimation of vertical gradients are mainly attributed to inaccurate emission and only partly to the transport uncertainties. However, large differences in model simulations are found over the regions/seasons of strong convection, which is poorly represented in the models. Overall, the zonal and latitudinal variations in CH₄ are controlled by surface emissions below 2.5 km and transport patterns in the middle and upper troposphere. We show that the models with larger vertical gradients, coupled with slower horizontal transport, exhibit greater CH₄ interhemispheric gradients in the lower troposphere. These findings have significant implications for the future development of more accurate CTMs with the possibility of reducing biases in estimated surface fluxes by inverse modeling.

Citation: Saito, R., et al. (2013), TransCom model simulations of methane: Comparison of vertical profiles with aircraft measurements, *J. Geophys. Res. Atmos.*, 118, 3891–3904, doi:10.1002/jgrd.50380.

Additional supporting information may be found in the online version of this article.

¹Research Institute for Global Change/JAMSTEC, Yokohama, Japan.

²Center for Atmospheric and Oceanic Studies, Tohoku University, Sendai, Japan.

³NOAA Earth Systems Research Laboratory, Boulder, Colorado, USA.

⁴Center for Global Environmental Research, National Institute for Environmental Studies, Tsukuba, Japan.

⁵Wageningen University and Research Centre, Wageningen, Netherlands.

⁶SRON Netherlands Institute for Space Research, Utrecht, Netherlands.

⁷Universite de Versailles Saint Quentin en Yvelines, Gif-sur-Yvette, France.

Corresponding author: P. K. Patra, Research Institute for Global Change/JAMSTEC, 3173-25 Showa-machi, Yokohama 236-0001, Japan. (prabir@jamstec.go.jp)

©2013. American Geophysical Union. All Rights Reserved.
2169-897X/13/10.1002/jgrd.50380

⁸European Centre for Medium-Range Weather Forecasts, Reading, UK.

⁹Atmospheric, Earth, and Energy Division, Lawrence Livermore National Laboratory, Livermore, California, USA.

¹⁰Goddard Earth Sciences and Technology Center, NASA Goddard Space Flight Center, Greenbelt, Maryland, USA.

¹¹Institute for Climate and Atmospheric Science, School of Earth and Environment, University of Leeds, Leeds, UK.

¹²School of GeoSciences, University of Edinburgh, Edinburgh, UK.

¹³Divisao de Quimica Ambiental, Instituto de Pesquisas Energeticas e Nucleares, Sao Paulo, Brasil.

¹⁴Cornell University, Ithaca, New York, USA.

¹⁵Centre for Australian Weather and Climate Research, CSIRO Marine and Atmospheric Research, Aspendale, Vic, Australia.

¹⁶Department of Geography and Environmental Studies Program, Western Michigan University, Kalamazoo, Michigan, USA.

¹⁷Center for Global Change Science, Massachusetts Institute of Technology, Cambridge, Massachusetts, USA.

¹⁸School of Chemistry, University of Bristol, Bristol, UK.

1. Introduction

[2] Methane (CH₄) is an important greenhouse gas, contributes to photochemical smog formation under polluted conditions by reaction with hydroxyl radical (OH), and is the main source of water vapor in the stratosphere [Graedel and Crutzen, 1993]. Over the last two decades, CH₄ simulations have been conducted using three-dimensional global chemistry transport models (CTMs) [e.g., Fung *et al.*, 1991]. Recently, a model intercomparison experiment (TransCom-CH₄) has been organized with the aim to assess the roles of uncertainties in model transport, surface emissions, and OH chemistry for simulating global CH₄. The first analysis [Patra *et al.*, 2011a] concentrated on background concentrations at the surface and showed overall consistent results across the participating models. However, that analysis was limited to eight surface sites, where simultaneous measurements of CH₄, sulfur hexafluoride (SF₆), and methyl chloroform (CH₃CCl₃) were available for more than 5 years in the period 1990–2007. Patra *et al.* [2011a] demonstrated that some models consistently underestimate or overestimate the meridional gradients of all the three species depending on the simulated rate of interhemispheric mixing. Based on SF₆ concentration gradients, for two northern (Barrow and Mauna Loa) and two southern (Cape Grim and South Pole) hemispheric sites, the interhemispheric exchange time is estimated to be in the range of 1.0–1.8 years for the suites of TransCom-CH₄ models.

[3] How the simulated zonal or meridional gradient varies with altitude for the long-lived species, however, has not been studied in detail yet. Nakazawa *et al.* [1991] suggested that the meridional gradient in the carbon dioxide (CO₂) concentration in the upper troposphere is significantly smaller compared to that near the Earth's surface. Stephens *et al.* [2007] showed that the CO₂ vertical gradients between the former suites of TransCom (Level 3) models, mostly developed pre-2000, varies widely due to the difference in vertical mixing rate. Note here that the interpretation of model transport has become complex using CO₂ due to strong seasonal variation in surface fluxes; strong source due to heterotrophic respiration in addition to fossil fuel emissions in the winter, and strong sink dominated by photosynthetic uptake in the summer [e.g., Miyazaki *et al.*, 2008]. The strong diurnal cycle in CO₂ fluxes also complicate flux-transport interaction vertically, particularly over the land region [Law *et al.*, 2008]. Because CH₄ sources dominate over the soil uptake on the surface in all seasons, and the atmospheric lifetime of CH₄ is about 10 years [Patra *et al.*, 2011a], the TransCom model intercomparison for CH₄ vertical profiles would be relatively straightforward for interpreting the transport and emission model errors. Advantages of using constituents (e.g., CH₄) with net sources on the Earth's surface over that of CO₂ to diagnose model transport have been shown over the South Asian region during the season of strong CO₂ uptake by the terrestrial ecosystem [Patra *et al.*, 2011b].

[4] Analyses of CH₄ vertical profiles using CTMs have been limited to single model [Bergamaschi *et al.*, 2009] and for specific regions [Beck *et al.*, 2012] and are proven to be useful for validating surface emissions. The TransCom-CH₄ data base includes simulated vertical profiles by 17 CTMs, which can be compared to data from several aircraft measurement programs that have been

carried out during the last decade [Tans *et al.*, 1996; Machida *et al.*, 2001; Gatti *et al.*, 2010]. The latitude-pressure distributions of zonal mean simulation results show that CH₄ concentrations, within the troposphere, decrease with altitude in the Northern Hemisphere (NH) and increase with altitude in the Southern Hemisphere (SH) [Patra *et al.*, 2011a]. Both the vertical and meridional gradients exhibit seasonal dependency in relation to seasonality in transport, surface emissions, or chemical loss. However, this conjecture is based only on the model intercomparison, without comparison with observations. Thus, an evaluation of the modeling results with aircraft observations will likely improve our understanding of CH₄ transport mechanisms of vertical and interhemispheric exchanges in the troposphere.

[5] The purpose of this study is to evaluate the simulated CH₄ concentrations using aircraft measurements. The model-observation difference depends on uncertainties in surface fluxes, model transport, and chemistry. We assess the flux and transport dependence of the model-observation differences using vertical profiles over a variety of surface conditions and transport regimes, e.g., wetlands in Siberia, tropical rainforests in Amazon, boreal forests of North America, and the marine environment. In the next sections, we briefly describe the model simulation scenarios and the aircraft measurement programs, followed by results and discussions. Some conclusions are given in section 4.

2. Models and Measurements

2.1. Simulation Concentrations

[6] The institutes participating in the TransCom-CH₄ experiment produced global CH₄ distribution using 13 models and four variants with different spatial resolutions and OH distributions. The CTM simulation outputs include CH₄ vertical profiles over various sites for a decadal period (1992–2007) with a 1 or 3 h time interval, for six CH₄ tracers that used different surface emission scenarios. A detailed description of the TransCom-CH₄ experiment is documented in Patra *et al.* [2011a]. In this study, we use CH₄ profiles simulated by 12 CTMs (Table 1), namely, the ACTM (atmospheric general circulation model-based CTM) [Patra *et al.*, 2009a, 2009b], CAM (Community Atmosphere Model) [Gent *et al.*, 2009], CCAM (Conformal-Cubic Atmospheric Model) [Law *et al.*, 2006], GEOS-Chem (Goddard Earth Observing System (GEOS) meteorology-driven CTM) [Fraser *et al.*, 2011], IFS (Integrated Forecasting System) [www.ecmwf.int/research/ifsdocs/CY36r1/index.html], IMPACT_1×1.25 (Integrated Massively Parallel Atmospheric Chemical Transport) [Rotman *et al.*, 2004], LMDZ (Laboratoire de Météorologie Dynamique—Zoom, version 4) [Hourdin *et al.*, 2006], MOZART (Model for Ozone and Related Chemical Tracers, version 4) [Emmons *et al.*, 2010], NIES08i (NIES CTM, version 2008 isentropic) [Belikov *et al.*, 2011], PCTM (Parameterized CTM) [Kawa *et al.*, 2004; Bian *et al.*, 2006], TM5_1×1 (Transport Model, version 5) [Krol *et al.*, 2005], and TOMCAT CTM [Chipperfield, 2006].

[7] These selected models used reanalyzed meteorology for simulating synoptic and shorter time scale (<7 days) variations in the observed time series. The newly participating

Table 1. List of the CTMs Used in This Study (See Text for Further Details) and Basic Model Features

Model Name	Contributing Institute	Vertical Levels	Horizontal Resolution	Source of Meteorology
ACTM	RIGC	67 σ	$\sim 2.8 \times 2.8^\circ$	NCEP2; U, V, T; SST
CAM	CU	28 σ	$2.5 \times \sim 1.9^\circ$	NCEP/NCAR
CCAM	CSIRO	18 σ	~ 220 km	NCEP; U, V; SST
GEOS-Chem	UoE	30/47 η	$2.5 \times 2.0^\circ$	NASA/GSFC/GEOS4/5
IFS	ECMWF	60 η	$0.7 \times 0.7^\circ$	ECMWF, ERA-interim
IMPACT_1 \times 1.25	LLNL	55 η	$1.25 \times 1.0^\circ$	NASA/GSFC/GEOS4
LMDZ	LSCE	19 η	$3.75 \times 2.5^\circ$	ECMWF; U, V, T; SST
MOZART	MIT	28 σ	$\sim 1.8 \times 1.8^\circ$	NCEP/NCAR
NIES08i	NIES	32 σ -0	$2.5 \times 2.5^\circ$	JCDAS, ERA-interim-PBL
PCTM	GSFC	58 η	$1.25 \times 1.0^\circ$	NASA/GSFC/GEOS5
TM5_1 \times 1	SRON	25 η	$1.0 \times 1.0^\circ$	ECMWF, ERA-interim
TOMCAT	UoL	60 η	$\sim 2.8 \times 2.8^\circ$	ECMWF, ERA-40/interim

IFS model is based on a semi-Lagrangian semiexplicit version of the European Centre for Medium-Range Weather Forecasts (ECMWF) spectral model (i.e., Eulerian vorticity-divergence configuration). The IFS model is run at the $0.7^\circ \times 0.7^\circ$ horizontal resolution, finest among all the participating models. The IFS model simulations of SF₆ and CO₂ has been found satisfactory in the TransCom continuous experiment [Law *et al.*, 2008].

[8] Five models, namely, ACCESS (The Australian Community Climate and Earth-System Simulator) [Corbin and Law, 2011] driven by climatological meteorology, ACTM_OH (OH sensitivity run of ACTM), GEOS-Chem_DOH (OH sensitivity run), IMPACT (low-resolution version), and TM5 (low-resolution version), are excluded

from main discussions of this analysis. For the control simulations, three-dimensional OH fields at monthly mean time intervals, based on Spivakovsky *et al.* [2000], have been prescribed in the TransCom-CH₄ protocol. Two of the models (ACTM and GEOS-Chem) repeated their TransCom runs with the same resolution and meteorology but with different OH fields. For both models, the vertical profile gradient was similar in the two different runs. The IMPACT and TM5 models repeated their TransCom runs using different horizontal resolution (implicitly different meteorology). For both models, we find relatively large differences, greater than the differences between different models, in some seasons. No clear distinction can be made whether the higher- or lower-resolution version of the

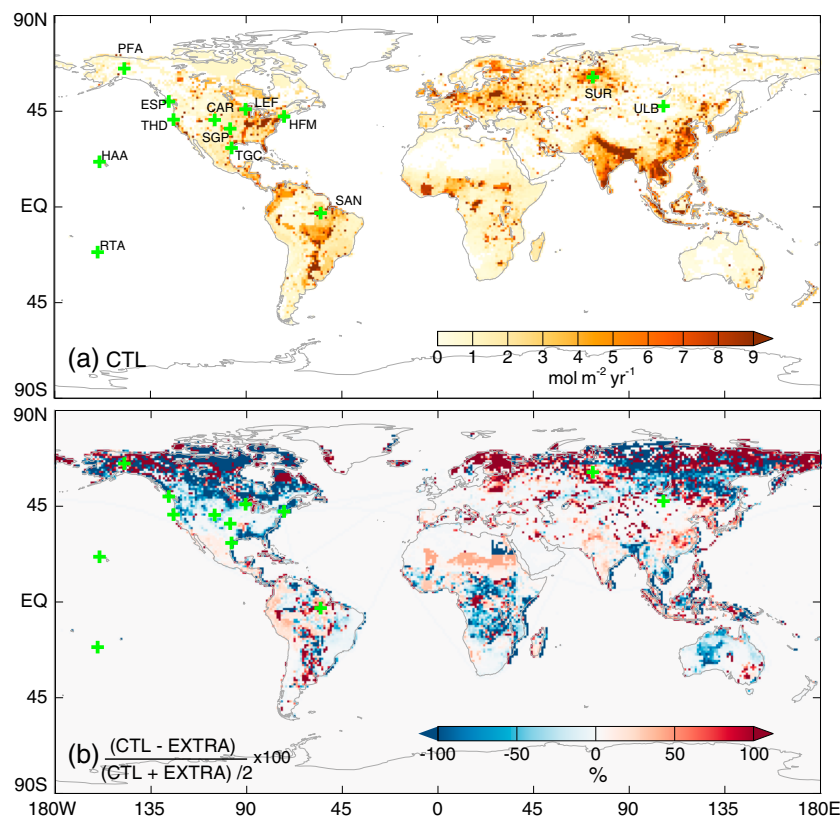


Figure 1. (a) Sampling locations for the aircraft measurements are overplotted on the map showing intensity of the annual mean CH₄ emission for the CTL flux. (b) Differences in emission distributions CTL and EXTRA.

Table 2. Site Details of the Aircraft Measurements Used in This Study^a

Site	Location	Latitude	Longitude	Above Mean Sea Level (m)	Period
PFA	Poker Flat	65.1°N	147.3°W	1200–7400	2001–2007
SUR	Surgut	61.0°N	73.0°E	500–7000	2001–2007
ESP	Estevan Point	49.6°N	126.4°W	300–5500	2002–2007
ULB	Ulaanbaatar	47.4°N	106.2°E	1500–6000	2004–2007
LEF	Park Falls	45.9°N	90.3°W	600–4000	2001–2007
HFM	Harvard Forest	42.5°N	72.2°W	600–7700	2001–2007
THD	Trinidad Head	41.1°N	124.2°W	300–7700	2003–2007
CAR	Briggsdale	40.9°N	104.8°W	2100–8700	2001–2007
SGP	Southern Great Plains	36.8°N	97.5°W	170–4900	2006–2007
TGC	Sinton	27.7°N	96.9°W	300–7700	2003–2007
HAA	Molokai Island	21.2°N	159.0°W	300–7700	2001–2007
SAN	Santarem	2.9°S	55.0°W	150–5200	2001–2005
RTA	Rarotonga	21.3°S	159.8°W	300–6100	2001–2007

^aThe Surgut site is operated by NIES, and all other sites are by the NOAA/ESRL.

models is better for these two models (see Figure S1 in the supporting information). However, earlier analysis has shown that the higher-resolution version of TM5 performs better than its coarser version for the interhemispheric gradients of SF₆, CH₄, and CH₃CCl₃ near the Earth's surface [Patra *et al.*, 2011a].

[9] We analyzed CH₄ tracers simulated using (1) the control emission scenario (CTL) (Figure 1) that combined seasonally varying natural sources (CYC NAT; major components being the emissions from biomass burning and wetlands) [see *Fung et al.*, 1991] and interannually varying anthropogenic emissions (ANT_IIV; based on EDGAR3.2) [see *Olivier and Berdowski*, 2001; *Patra et al.*, 2009a for details] and (2) the EXTRA flux, in which interannually varying biomass burning emissions are based on GFEDv3 [*van der Werf et al.*, 2006] and wetland emissions are from the VISIT terrestrial ecosystem model [*Ito and Inatomi*, 2012]. Based on our experiences in *Patra et al.* [2011a], these two tracers are sufficient to evaluate the differences in the simulations caused by the emission distribution and strength. The CTL and EXTRA emissions differ by more than 100% over some of the regions (Figure 1b). To remove systematic offsets between the CTM simulations, the decadal mean concentrations in the altitude range of 2–6 km over Hawaii (HAA) is subtracted from the simulation results. This implies that the horizontal gradients between sites can be studied in reference to Hawaii, but the offset treatment does not affect the determination of vertical gradients or other parts of analysis. For all statistical calculations, the model values are sampled at the time and location of the observations. Model values, between the vertical layers below and above their respective coordinates, are linearly interpolated to measurement height.

2.2. Aircraft Measurements

[10] Vertical CH₄ profiles have been measured using small aircraft by the National Oceanic and Atmospheric Administration (NOAA) Earth System Research Laboratory (ESRL) at sites in North America and the Pacific (www.esrl.noaa.gov/gmd/ccgg/aircraft/index.html), by the National Institute for Environmental Studies (NIES) at a site in Siberia [*Machida et al.*, 2001], and by NOAA/ESRL in collaboration with Instituto de Pesquisas Energéticas e Nucleares at sites in Amazon [*Gatti et al.*, 2010]. The site names are listed in Table 2, and their locations are plotted

with green symbols on a global CH₄ emission map in Figure 1a. Air samples are collected using aircraft in the altitudes from the Earth's surface up to 4–10 km depending on the site (Table 2). The aircraft measurements are conducted a few times a month with measurements continuing to the present for all sites, except for Amazon (SAN), where they terminated in 2005. The observation period for each site overlapping with our analysis period is shown in Table 2. Only 2 of the 13 sites are located in the Southern Hemisphere, and 8 of the 11 sites in Northern Hemisphere are located in and around the North American continent. Thus, our analysis of vertical and horizontal gradients does not cover the globe as uniformly as desired for evaluating vertical and horizontal gradients in CH₄ and other trace gases.

[11] The samples collected over Surgut, Russia, are analyzed using gas chromatography (Agilent 5890, Agilent Technologies, Inc.) equipped with a flame ionization detector (GC-FID) calibrated against the NIES-94 CH₄ scale. The analytical precision of the GC-FID for the CH₄ concentration was estimated to be less than 2.0 ppb. The NIES-94 CH₄ scale is higher than the WMO (NOAA-04) scale by 3.5–4.6 ppb in the concentration range of 1750–1840 ppb [*Zhou et al.*, 2009]. To account for the calibration scale difference, an average value of 4 ppb is subtracted from the measurements over Surgut.

[12] The NOAA ESRL aircraft measurements are made by collecting air samples in 0.7 L silicate glass flasks at biweekly to monthly intervals at about 16 sites on a regular basis and on campaign mode over Santarem, Brazil (Table 2). Air samples are collected using a turboprop aircraft in the altitude range of about 500 m to 8 km. CH₄ is measured by GC-FID at accuracy of ±1.2 ppb. The concentrations are reported at the absolute calibration scale of NOAA-04 that is maintained as the WMO standard [*Dlugokencky et al.*, 2005].

3. Results and Discussions

[13] We compare the CTM simulation results with the aircraft measurements to understand the differences between the models and evaluate performance of the models in comparison with measurements during the analysis period of 2001–2007.

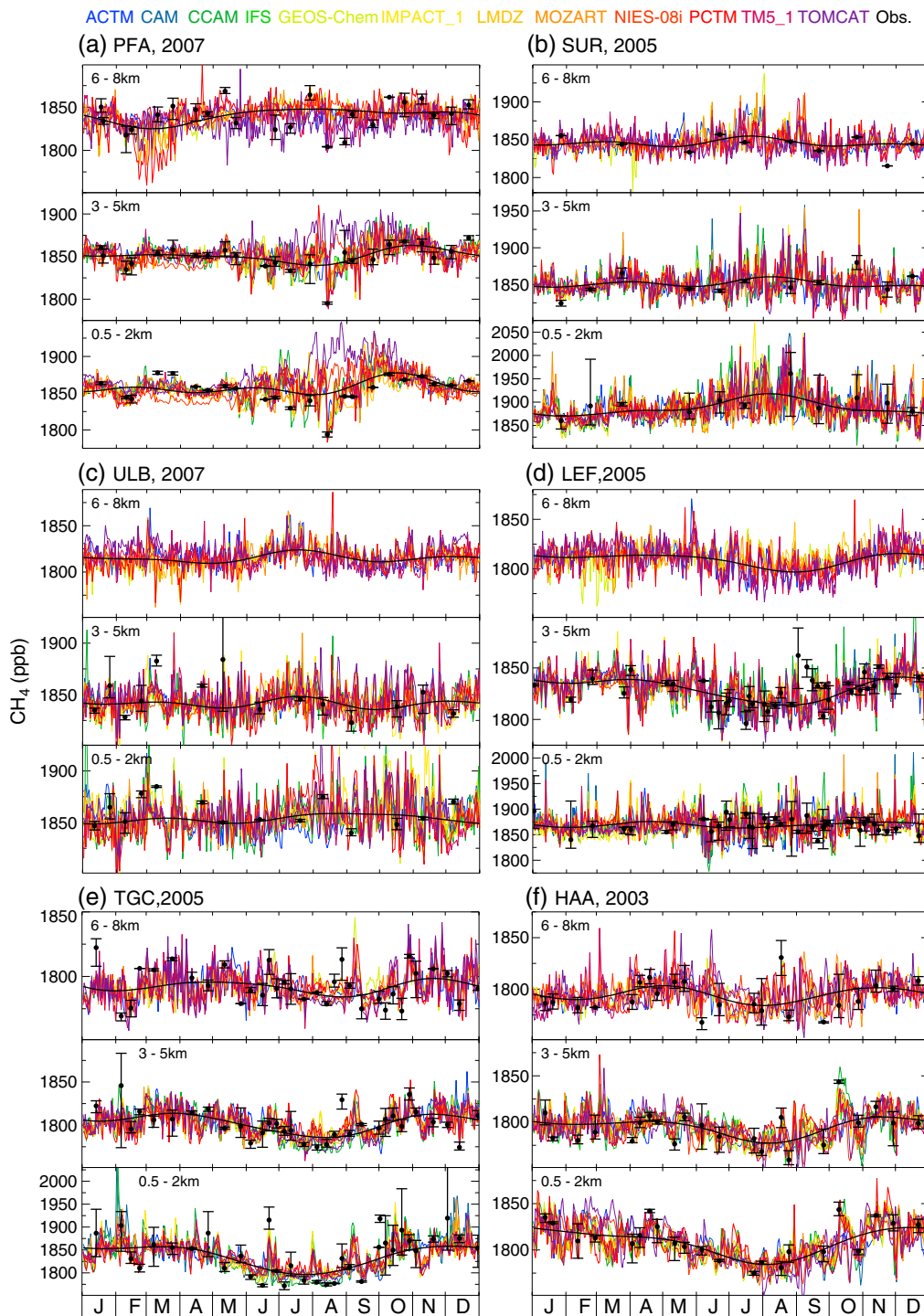


Figure 2. Seasonal variations of the observed (black dots with error bar) and simulated (color lines; see legends at the top; continuous at daily intervals) CH₄ concentrations are shown for a comparison at selected sites (time period differs based on data availability at sites, and y axis range differs to show detailed variability). The error bars show the 1 σ standard deviation of all data within a selected height range. Smooth black lines present fitted curves (three harmonics) to the average seasonal cycle for all the models. The results for each site are averaged over three different altitude ranges, representing lower troposphere (0.5–2 km), middle troposphere (3–5 km), and upper troposphere (6–8 km).

3.1. Seasonal and Daily Variations at Different Heights

[14] Figure 2 shows the observed and simulated time series of CH₄ concentration for 2007 for three different

height ranges (0.5–2, 3–5, and 6–8 km) and six sites. Information on seasonal cycles is sometimes difficult to extract from the measurements given the irregularity in data coverage and gaps in the time series (black dots). For better

Table 3. Measured and Model Simulated Seasonal Cycle Amplitudes of CH₄ at Two Altitude Ranges^a

Sites	1–3 km			3–5 km		
	Observed	Model		Observed	Model	
		Mean	SD		Mean	SD
PFA	28.9	31.6	7.5	28.9	24.6	4.7
SUR	56.4	49.9	16.9	39.5	18.6	5.1
ESP	34.9	40.1	4.5	33.4	24.2	6.9
ULB	35.0	20.5	6.7	35.2	16.2	3.3
LEF	32.4	27.5	6.5	32.9	30.2	5.1
HFM	48.9	26.8	7.0	34.6	28.8	6.6
THD	42.3	38.8	4.7	29.2	29.3	6.2
CAR	–	–	–	34.7	30.0	8.8
SGP	73.9	52.1	14.7	38.7	32.3	5.7
TGC	89.0	65.1	13.7	32.9	26.1	7.0
HAA	36.9	44.0	8.6	30.2	34.8	4.5
SAN	86.7	46.9	10.0	68.6	33.3	7.2
RTA	26.4	28.3	12.9	35.1	25.2	6.8

^aModel results are given as mean and 1 σ standard deviations (individual model results are available in Table S1).

clarity, we only show multimodel mean seasonal cycles (black line), which are created by fitting a curve (three harmonics) to the afternoon (1200–1600 h local time) mean time series. This method ensures unambiguous identification of the peaks and troughs in the simulated seasonal cycles of CH₄, which is otherwise not well defined due to large data gaps at some of the observation sites. The amplitude and phase of the simulated seasonal cycles are similar for most models, e.g., except TOMCAT, at the northernmost site (PFA). Although the synoptic and daily scale variations show differences between the modeling results, we find that the observed seasonal cycle matches the models within 1 σ standard deviations at most sites (Table 3). The observed seasonal cycle is significantly different from the model mean seasonal cycles for some of the continental/coastal sites (ULB, HFM, TGC, and SAN) at 1–3 km height, where the uncertainties in both surface emissions and model transport are greater compared to those at the remote marine site. The synoptic variations (2–10 day) are consistent between models (correlation coefficients generally greater than 0.5; Table S1), indicating similarities in reanalyzed meteorological parameters used in the models. While the behavior of seasonal cycles depends on temporally varying regional emissions and seasonality in zonal mean OH radical, the synoptic variations in CH₄ are produced by regional patterns of emissions and model transport variability at the synoptic time scale. Therefore, we conclude that the synoptic transport and CH₄ emission distribution are fairly well represented in all models.

[15] The peak-to-trough seasonal cycle amplitude at 1–3 and 3–5 km height ranges for SAN, TGC, SGP, and SUR are relatively large compared with the other sites (Tables 3 and S1). Greater daily CH₄ variations during summer are simulated at SUR, PFA, LEF, and ULB near the surface, coinciding with the seasonal maximum of CH₄, and are thought to be caused by the increase in surface emissions in summer and the seasonally varying dynamics associated with the planetary boundary layer (BL) height as well as cumulus convection. On the other hand, troughs of the multimodel mean seasonal cycles at TGC, HAA, and the other remote sites sampling background air show lower variability during

the boreal summer months, coinciding with the seasonal minimum of CH₄ in the troposphere, except for RTA. In general, the seasonal amplitudes in the lower troposphere are similar to or larger than those in the upper troposphere. The seasonal amplitude at the northern central Pacific site HAA decreases from 36.9 to 30.2 ppb with altitude, whereas the seasonal amplitude at the southern central Pacific site RTA increases from 26.4 ppb at 1–3 km to 35.1 ppb at 3–5 km (Table 3). Throughout the Northern Hemisphere, the amplitude weakens upward as the emission signal from the lower troposphere propagates to the middle/upper troposphere. This weakening is especially remarkable at TGC (Figure 2e), where the CH₄ seasonal cycle amplitude at the 6–8 km range is reduced to 11% of that at 0.5–2 km (all model average of 79 ppb). On average, the amplitude decreased only marginally at ULB, PFA, ESP, and LEF, while at other sites, the amplitude decreased between 30% and 60% at 6–8 km compared to that at 0.5–2 km. Note here that the anthropogenic or biogenic emissions around the Mongolian site ULB is among the lowest observed over the land regions, while PFA, ESP, and LEF are located around the regions of strong CH₄ emissions during the boreal summer.

[16] One unusual feature among the seasonal cycles is observed as an increase in CH₄ at 6–8 km height over SUR (73°E, 61°N) during May–July. The timing of this peak in June–July at 6–8 km is ahead of the seasonal peak seen near the surface (0.5–2 km) in July–August, and there is almost no seasonal variation in the 3–5 km altitude. An examination of CH₄ longitude–pressure cross sections (latitude range: 60°N–65°N; Figure S2) suggests that the high CH₄ over SUR during the late spring/early summer is transported from Western Europe. Air masses carrying the signature of European emissions are lifted over the Ural mountain range (57°E, 51°N to 66°E, 68°N) and are subsequently transported to Siberia, Mongolia, and as far as western North America by the prevalent westerly winds, as suggested by the longitude–pressure cross sections of CH₄ concentrations (Figure S2). The CH₄ peak near the surface is coincident with the seasonal high in emissions from the wetlands in the Siberian region.

3.2. Vertical Profiles

[17] Figure 3 shows the seasonal mean vertical CH₄ profiles at SUR, TGC, HAA, and SAN with the CTL fluxes during boreal winter (January–March: JFM) and summer (July–September: JAS). The modeled (color lines) and observed (black dots with horizontal bars) vertical profile variations with altitude agree well, inside the standard deviation (black bars) of the seasonal variation of the observed CH₄ concentrations.

[18] The simulated vertical profiles at SAN show larger differences between models (a spread of 50 ppb at all altitudes) and with measurements. Due to sparse measurements at some of the sites, e.g., SAN, the significance of model–observation differences cannot be assessed here, and the altitude range is limited to below 4 km. CH₄ concentrations near the surface are affected by biospheric or anthropogenic activities (including biomass burning) as well as meteorological conditions. For example, clear synoptic variability is observed near the surface at TGC during the JAS months as the site is either under the influence of marine air from

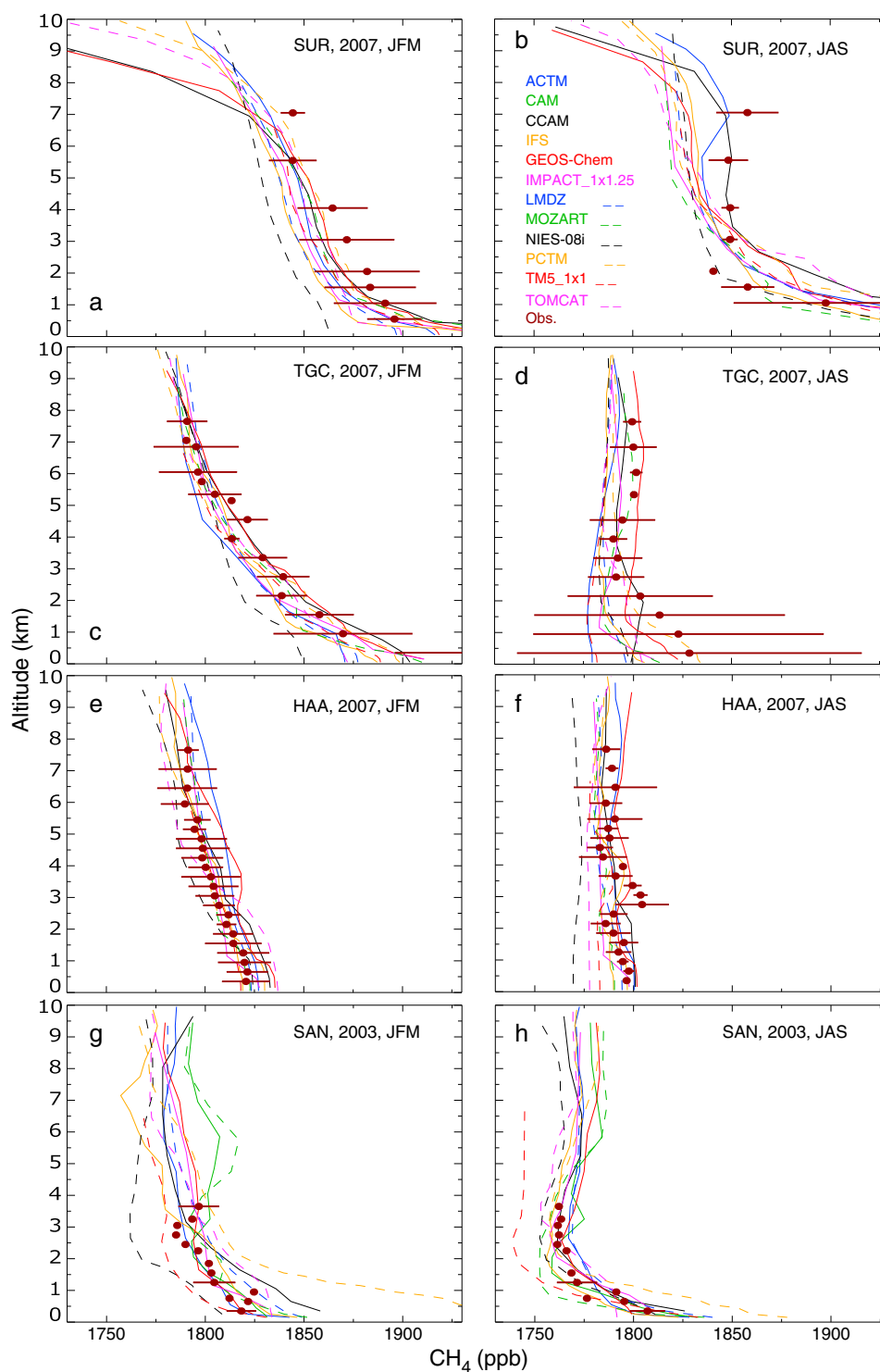


Figure 3. (symbol) Observed and (lines) simulated CH₄ vertical profiles at (top row) SUR, (second row from top) HAA, (third row from top) TGC, and (bottom row) SAN for (left) January–March and (right) July–September. Horizontal bars for the 3 months mean measurements present a 1 σ standard deviation. Results for 2005 and 2007 at more number of sites are shown in Figure S3 (observations at SAN are available only in 2003).

the Atlantic Ocean from the southeast (seen as relatively low concentrations) or from regional emission hot spots around the Gulf of Mexico. During the JFM months, winds are predominantly southwesterly, and the TGC site is under

the influence of emissions in Mexico and southwestern United States. Thus, the concentrations are relatively stable (lower variability), and the average values are higher by about 50 ppb in JFM months than those in the JAS months.

This is due to slower chemical loss of CH₄ by OH in JFM compared to the JAS months in this latitude band.

[19] At SUR, except below 2 km, the simulated results are generally lower than the observed CH₄ concentrations during both seasons. A more contrasting feature is observed in the JAS season when the measurements show slightly increasing or fairly constant CH₄ concentration between 2–3 and 7–8 km at SUR (and also at TGC). Such elevated levels of gases in the upper troposphere (7–8 km altitude), with emissions only on the Earth's surface, occur frequently in the presence of deep cumulus convection [e.g., *Patra et al.*, 2009b] (refer also to Figure S2 for the cross-sectional view over Siberia). Only ACTM and CCAM simulations capture this feature to some extent over SUR. This is a clear indication that 10 out of 12 models underestimate vertical transport of surface emissions to the upper troposphere over Surgut due to deep cumulus convection during the JAS season. As discussed earlier, the higher CH₄ values during May–June were under the influence of emissions over the Western Europe.

[20] The concentration at SAN sharply decreases with altitude in the lower troposphere, suggesting significant CH₄ emission at this location, and the profiles above 3 km are relatively straight or slightly increasing in both seasons, indicating strong vertical motion in all seasons over this tropical site (Figures 3g and 3h).

[21] When the convective activity is intense during the boreal summer, relatively straight vertical profiles are also observed at HAA, TGC, and other NH sites. The profiles at ocean sites HAA and RTA usually reveal characteristics of a background site with insignificant surface emissions around the site during all seasons. However, emission signals from Equatorial Asia/Western Pacific and Temperate Asia reach HAA during October–January and April–July, respectively, at 850 hPa altitude (Figure S2). In addition, the Hawaiian Islands are located at the subtropical mixing barrier for chemical species [*Miyazaki et al.*, 2008], causing greater seasonal variability at HAA than RTA in the lower troposphere (Table 3). Thus, the vertical profiles at HAA show a gradient in the JFM months despite being an ocean site due to the influence of northern hemispheric emissions and weak OH loss (Figure 3e).

[22] The CH₄ peak at 3–4 km during the JAS months over HAA (Figure 3f), typical of all years, is caused by the transport of high CH₄ from Boreal Asia along the isentropic surfaces when the convective activity is low. Four models (GEOS-Chem, PCTM, IFS, and TM5) are able to simulate this feature to some extent. GEOS-Chem and PCTM are driven by the meteorological reanalysis from the Goddard Earth Observing System Data Assimilation System, whereas IFS and TM5 use ERA-Interim meteorology from the European Centre for Medium-Range Weather Forecasts (ECMWF). It is however unclear whether the better simulations by four models using GEOS and ECMWF reanalysis are due to the quality of meteorological products or from the representation of transport in the models. Sensitivity simulations using one of the models with both reanalysis products are needed to address this issue.

3.3. Differences Between the Observations and Model Simulations

[23] Figures 4a–4d show the model-observation scatterplots at four different height ranges (black: 0.5–1.5 km, blue:

1.5–3.0 km, green: 3.0–5.0 km, and red: 5.0–7.0 km) at sites SUR, THD, SGP, and HAA. The black diagonal line intersects at the coordinate origin with slope 1. Correlation coefficients R between the model and observation time series are presented in Table S1. Several values, denoted by “0,” did not satisfy a significance level of 0.05 based on the critical value for testing the null hypothesis H_0 of noncorrelation between two time series. Higher correlation coefficients in 3–5 km altitude range than that at 1–3 km altitude range suggest that the variance of model-observation difference is larger near the surface than in the free troposphere at most sites. This is primarily due to large emission signals as well as greater site representation error near the Earth's surface at synoptic time scales. These emissions are uncertain (e.g., monthly averages are used), which leads to larger model error near the surface. In contrast, the signals in the midtroposphere are dominated by transport processes.

[24] Figures 4e–4h shows the frequency distribution of the model-observation difference at different seasons in winter (black: JFM), spring (blue: AMJ), summer (green: JAS), and autumn (red: OND) for the analysis years of 2001–2007. The model-observation difference at HAA in Figure 4h (also CAR, RTA, and ULB) falls within a small range of CH₄ concentrations (± 15 ppb, 1σ), and has a higher correlation (generally greater than 0.7 in Table S1, except NIES08i and TOMCAT) than at the other sites because of their location in the background marine environment (RTA and HAA) and inland (CAR and ULB) away from direct influence of continental sources (Figure 1). The model-observation differences at SUR, SGP, and THD (also SAN, LEF, HFM, and PFA) are as large as 100 ppb for the high CH₄ concentrations near the Earth's surface (Figure 4).

[25] The frequency distribution for the small model-observation mismatches in the regions around HAA (Figure 4h), CAR, RTA, and ULB (not shown) shows little or no skewness. The low (high) skewness indicates small (large) seasonally varying model biases, while high kurtosis suggests that the model time series is well correlated with the observation time series. The skewness at THD is also small, and the kurtosis is low compared with the Gaussian distribution that is symmetric around 0 difference. On the other hand, SGP shows negative skewness, and the peaks of the population densities in spring and summer (blue and green histograms in Figure 4g) are negatively biased by about 20 ppb. Thus, Figures 4c and 4g confirm that the models simulated relatively low CH₄ concentrations compared to the observations at SGP. At SUR, the peak in summer (green in Figure 4e) is marginally skewed positive due to an overestimation of the modeled CH₄ concentrations. These results suggest that the used CTL CH₄ emissions are too low (marginally high) around the SGP (SUR) site.

[26] These biases in simulated CH₄ concentrations are unlikely to be due to transport model errors, because most models systematically show similar underestimations/overestimations, and the performance of the TransCom-CH₄ model ensemble has been found to be satisfactory at all other sites (e.g., Figures 4f, 4h, and S3). In addition, the lifetime of atmospheric CH₄ is longer than 1 year in the troposphere, much longer compared to the transport or emission time scales around any given location [*Patra et al.*, 2009a]. Thus, the model biases between sites within a hemisphere/continent are not likely to arise from uncertainty

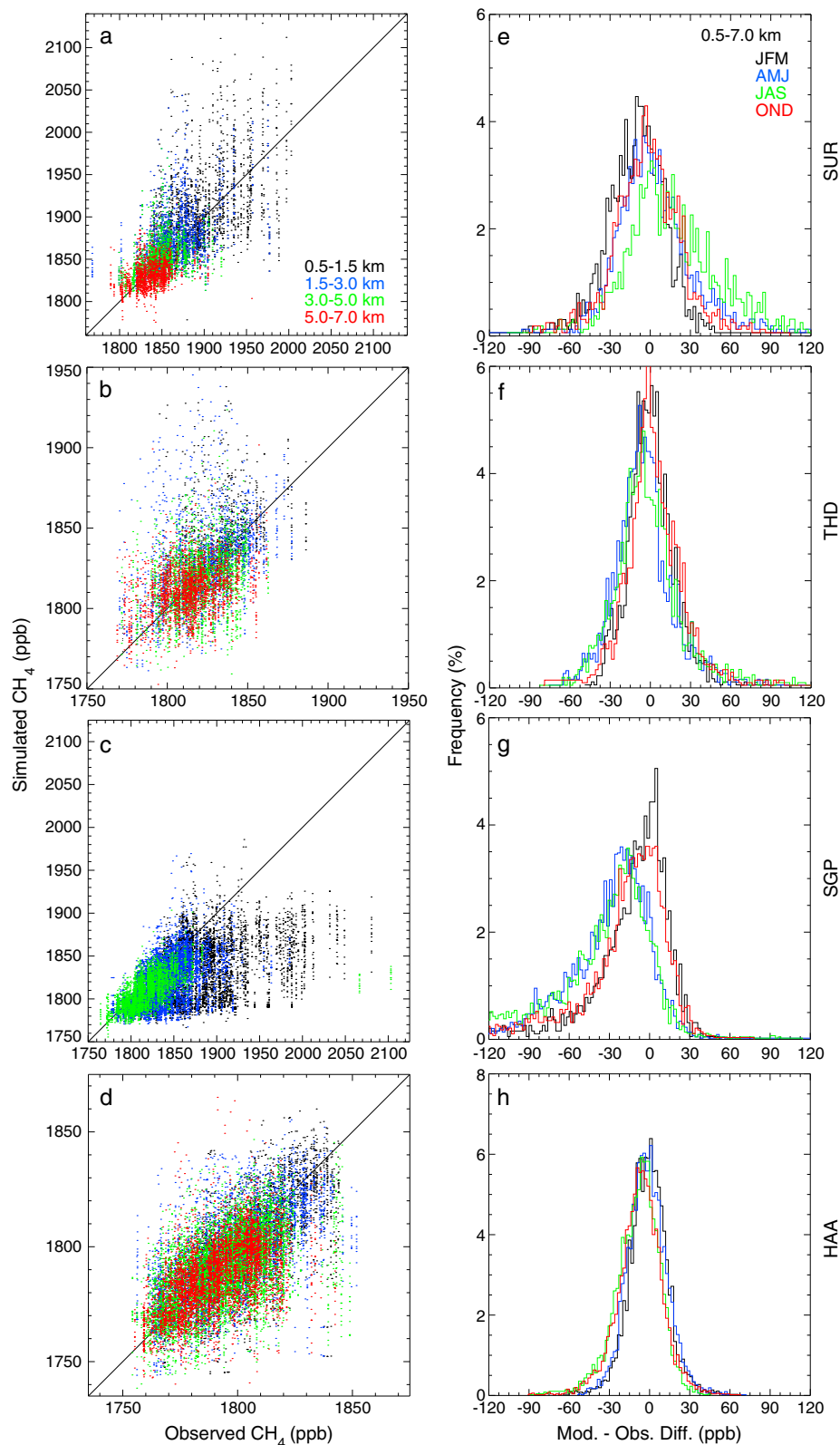


Figure 4. Correlations of observed and simulated CH₄ concentrations for the analysis period (2001–2007) for four selected sites (SUR, THD, SGP, and HAA are organized from top to bottom row, respectively). The symbols within each panels of the left column correspond to different heights: (black) 0.5–1.5, (blue) 1.5–3.0, (green) 3.0–5.0, and (red) 5.0–7.0 km. Note that the axis range varies for Figures 4a–4d. The right panels show the frequency distribution of model-observation differences, averaged over all the CTMs and the altitude range 0.5–7.0 km for different seasons of (black) JFM, (blue) AMJ, (green) JAS, and (red) OND, where the class interval is 2 ppb.

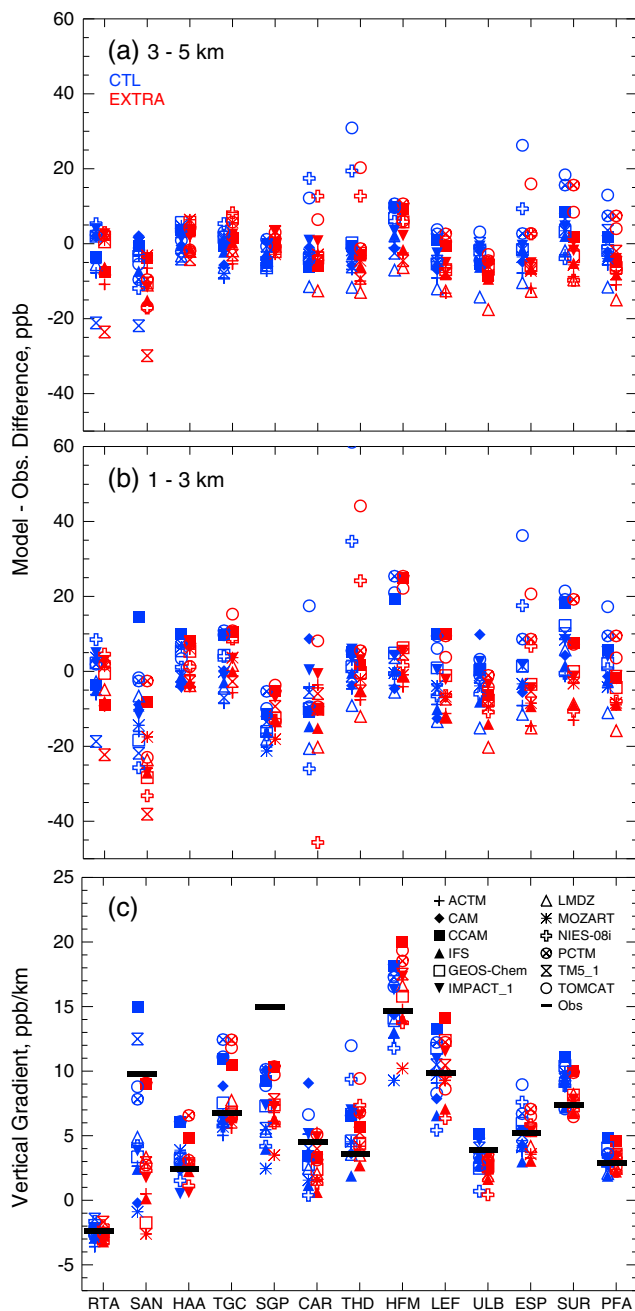


Figure 5. Differences between the observed and simulated CH₄ concentrations averaged for the analysis years (2001–2007) are shown for the (a) middle troposphere (3.0–5.0 km) and (b) lower troposphere (1.0–3.0 km). All values are offset by the yearly average CH₄ concentrations over 1–6 km at HAA before calculating the differences. Results corresponding to CTL and EXTRA fluxes are shown in blue and red, respectively. (c) Vertical gradients of the CH₄ concentrations between 1–3 km and 4–6 km altitude ranges.

in OH abundance. Figures 5a and 5b show mean model-observation differences due to two emission scenarios used in this analysis, CTL (blue symbols) and EXTRA (red symbols), in the middle and lower tropospheric altitudes. Smaller model-observation differences are found at SUR in the EXTRA simulations, which has lower CH₄ emissions

compared to CTL case in the Siberian region (Figure 1b). This suggests that the CTL CH₄ emissions around SUR are too high. Model simulations using either CTL or EXTRA emissions underestimate the observed CH₄ concentrations at SAN, suggesting stronger emissions from the Amazon region or the vertical transport is faster in the models.

3.4. Vertical, Latitudinal, and Longitudinal Gradients

[27] We show the annual mean simulated and observed vertical gradients in Figure 5c and Table S2. Here the vertical gradient in CH₄ profiles is defined as the difference of concentrations between the 1–3 km and 4–6 km heights.

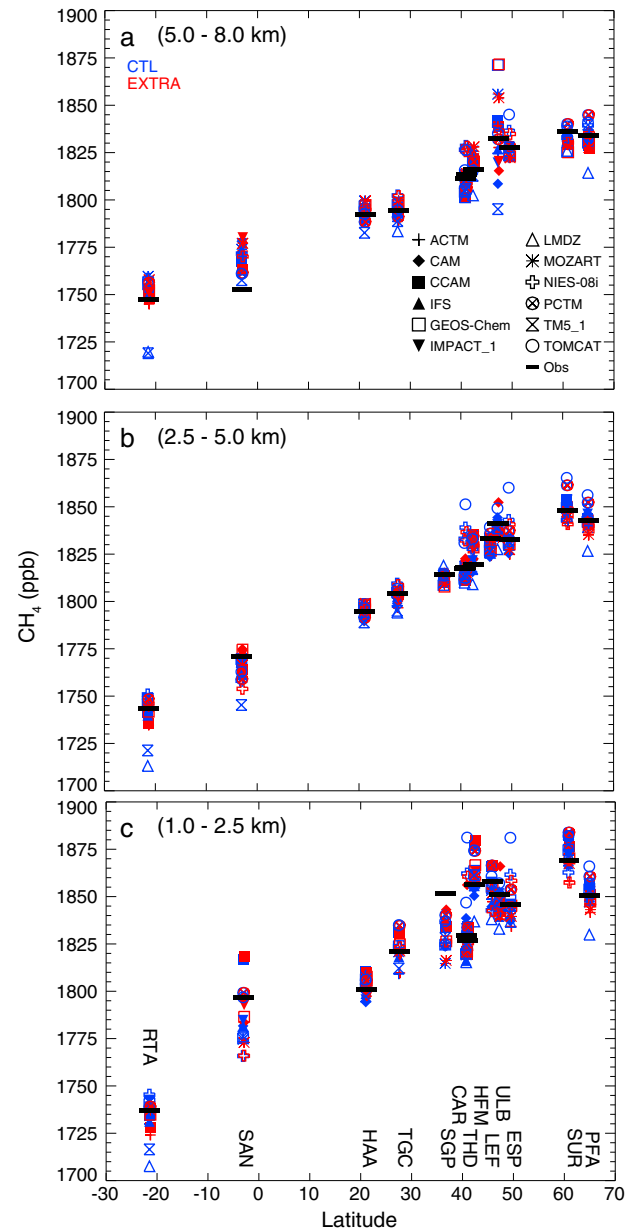


Figure 6. The CTM-simulated CH₄ concentrations averaged in the (a) upper troposphere of 5.0–8.0 km, (b) middle troposphere of 2.5–5.0 km, and (c) lower troposphere of 1.0–2.5 km for the analysis years (2001–2007) with the (blue) CTL and (red) EXTRA fluxes and (black) observed concentrations.

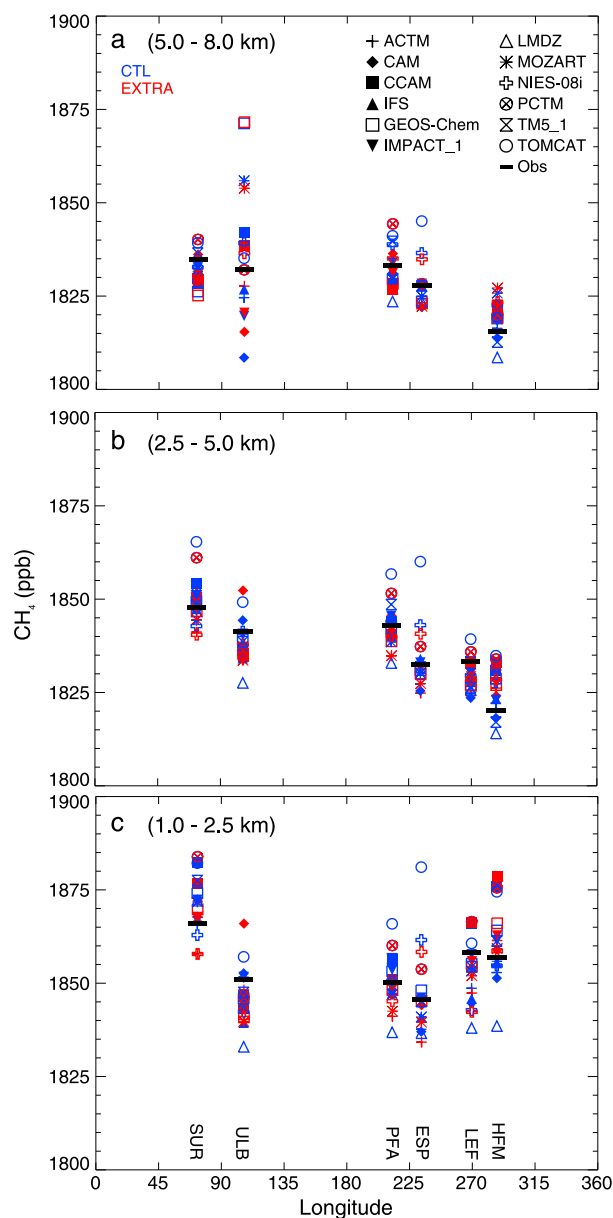


Figure 7. Longitudinal distribution of the CTM-simulated CH₄ concentrations at sites higher than 42°N (i.e., SUR, ULB, PFA, ESP, LEF, and HFM from 0°E to 360°E), averaged in the (a) upper troposphere of 5.0–8.0 km, (b) middle troposphere of 2.5–5.0 km, and (c) lower troposphere of 1.0–2.5 km for the analysis years (2001–2007) with the (blue) CTL and (red) EXTRA fluxes and (black) observed concentrations.

The simulated vertical gradients are generally within 5 ppb of the observed gradients at the oceanic sites (i.e., RTA and HAA), most of the coastal sites (i.e., TGC, ESP and PFA), and some of the continental sites (i.e., CAR, SUR, and ULB). The differences between simulated and observed vertical gradients are more than 5 ppb at SAN, SGP, LEF, and HFM (continental sites). The model-observation differences are systematically biased positive and negative, respectively, at SUR/THD and SAN/SGP, for most of the transport models. These results are consistent with overestimation and underestimation of simulated concentrations compared

to observations in the lower troposphere at SUR and SGP, respectively (Figures 4a and 4e and Figures 4c and 4g). These systematic model-observation biases are thus likely to be caused by regional emissions in the CTL scenario rather than errors in CH₄ loss (longer than 1 year lifetime due to OH reaction) and model transport. By using EXTRA emissions (red symbols), the simulated vertical gradients worsen for the sites SAN, HFM, and ULB, in comparison with the observations, but improve slightly over SUR.

[28] Figure 6 shows comparisons of the simulated and observed latitudinal distributions of CH₄ concentrations among all sites at different height ranges (1.0–2.5, 2.5–5.0, and 5.0–8.0 km). The measured CH₄ concentrations increase from SH to NH between 20°S and 50°N in the troposphere, at near linear rates of 1.4 ppb/deg at 1.0–2.5 km, 1.3 ppb/deg at 2.5–5.0 km, and 1.2 ppb/deg at 5.0–8.0 km. These values are generally well simulated by the models using both CTL and EXTRA emission scenarios. The differences in latitudinal gradient are mainly due to the decrease in CH₄ concentrations with height in the NH, e.g., the upper tropospheric concentration in the NH high-latitude sites is ~30 ppb lower than the lower tropospheric values. The agreement between model and observations is best for the 2.5–5.0 km altitude range, where the standard deviation of model-observation differences is ~5 ppb (see also Table S3). Although model uncertainty in the free troposphere is usually small, variance among the models at ULB at 5 Alkm is larger than that in the other sites. This is presumably due to the long-range transport of European and Siberian CH₄ emission signals to ULB as discussed earlier (section 3.1). The smaller (1.2 ppb/deg) interhemispheric gradient at 5intkm, compared to that at 2.5–5.0 km heights, indicates that the CH₄ in the NH upper troposphere is more readily transported to the SH. This effect can be seen as the higher CH₄ concentration in the upper troposphere at RTA than in the lower troposphere. A higher concentration in the SH upper troposphere compared to that in the lower troposphere is also observed for nonreactive species, such as CO₂ and SF₆ [Nakazawa *et al.*, 1991; Miyazaki *et al.*, 2008; Patra *et al.*, 2009b; Sawa *et al.*, 2012]. The role of surface emissions on meridional gradient weakens rapidly with increasing height between 1.0–2.5 and 2.5–5.0 km (Figures 6b and 6c).

[29] Figure 7 shows the variation of CH₄ with longitude for sites north of 42°N (i.e., SUR, ULB, PFA, ESP, LEF, and HFM) in the same height ranges as Figure 6 in order to investigate zonal CH₄ transport and vertical propagation driven by surface CH₄ emissions from North America, Europe, and Siberia. The lower tropospheric variations in CH₄ are mainly linked to stronger emissions around SUR and HFM compared to those around ULB and ESP. The CH₄ concentrations in the middle troposphere clearly have an eastward decreasing trend in observation and models for both CTL and EXTRA emissions (about –0.1 ppb/deg from the prime meridian to eastward; Figure 7b). The high CH₄ concentration in the lower troposphere over Siberia (Figure 7c) is diluted through mixing and reduces the difference between average values at SUR and other sites (except HFM) at the 5–8 km height range (Figure 7a). This behavior is seen consistently for measurements and model using both the emission scenarios. Apparently, the CH₄-rich air over the Eurasian continent in the upper troposphere

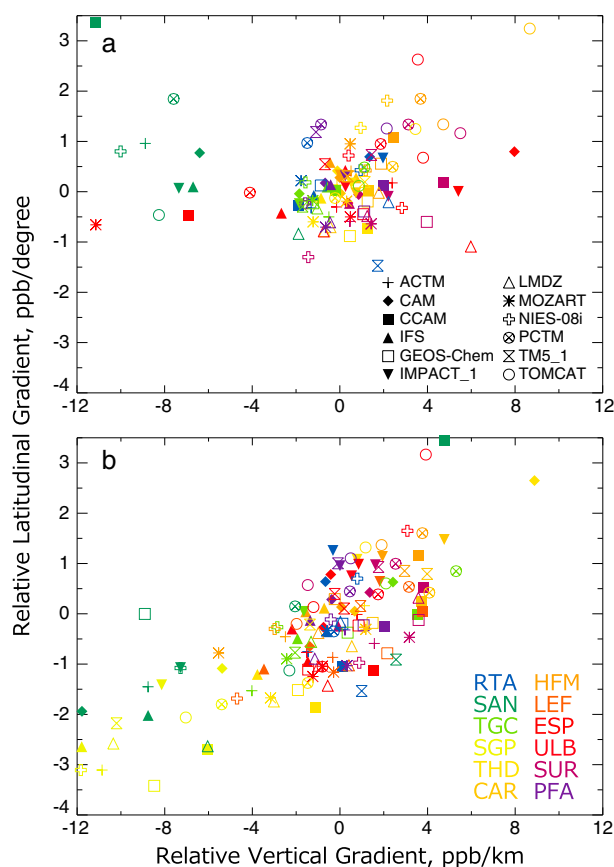


Figure 8. CH₄ vertical gradients (ppb/km) are plotted against the latitudinal gradients in CH₄ (ppb/deg) between the sites within two altitude ranges: (a) 3.0–5.0 km and (b) 0.5–2.5 km. All data are averaged for the period 2001–2007, and the results for the CTL flux are shown. The symbol for each model is color-coded for the gradients between each site and the reference site HAA. Both gradients are plotted as a difference relative to the measured gradients.

extends to the western side of the North American continent (PFA and ESP) as suggested by the longitude-pressure cross-sectional plots (refer to Figure S2). The air in the upper troposphere on the eastern side of northern United States mostly originates at about 40°N over the Pacific Ocean, except for the winter months, giving relatively low CH₄ concentrations at HFM. These results are generally consistent with Xiong *et al.* [2010], but our understanding is improved significantly on the longitudinal variations in upper tropospheric CH₄ by including a greater number of vertical profile measurements.

3.5. Correlation of Latitudinal and Vertical Transports

[30] The overestimations or underestimations of latitudinal gradients of long-lived atmospheric species simulated by models, compared to the measurements, are thought to be linked with the vertical concentration gradients of those species [Denning *et al.*, 1999]. To explore this hypothesis further, we show scatterplots of vertical gradients at each site and latitudinal gradient, with reference to HAA, within two altitude ranges 3–5 and 0.5–2.5 km (Figure 8). Both gradients are plotted as the differences relative to the measured gradients, showing which models overestimate

or underestimate the vertical and latitudinal gradients. Relative gradients are chosen to remove biases in simulated concentrations with respect to measurement, which are often greater than the measured gradients. In the middle troposphere (3–5 km), relative vertical and latitudinal gradients are scattered in the approximate ranges of -10 to $+7$ ppb/km and -1.5 to $+2.0$ ppb/deg, respectively. Loose correlation between vertical and horizontal gradients suggests that the interhemispheric transport is relatively insensitive to the local/regional vertical profile of CH₄ in the 3–5 km altitude range and that the transport in the models is similar. However, the relative latitudinal gradients are apparently proportional to the relative vertical gradient in the lower troposphere (0.5–2.5 km), suggesting that the vertical transport of emission signals through the lower troposphere plays a critical role in determining interhemispheric gradients near the Earth's surface.

[31] A schematic representation of the relationship between vertical and interhemispheric transports is shown in Figure 9a. The monthly mean modeled vertical gradients in the NH are calculated as the difference between the CH₄ concentrations between 900 and 500 hPa altitudes. Values are also averaged over all the model grid cells between 30°N and 50°N for 2007. Average latitudinal gradients are calculated as the difference between mean CH₄ for SH (50°S–30°S) and NH (30°N–50°N). Annual mean values of the interhemispheric and NH vertical gradients in CH₄ show a compact relationship (black symbols). The seasonal variations in this relationship are mainly controlled by the vertical transports and the emission and loss rates of CH₄. In July, both the latitudinal and NH vertical gradients are smaller than those in the other seasons because of faster loss rates in the NH and lower loss rates in the SH as well as stronger vertical mixing in the NH, despite high emission rates in the NH. In October, the NH vertical gradients are the largest among all seasons (high emission rate, low loss scenario), although the latitudinal gradients do not increase significantly. In January, the midtropospheric CH₄ concentrations reach a seasonal high because of accumulation in the NH through autumn and early winter (low emission, very low loss scenario, and weaker vertical mixing). This condition leads to the largest interhemispheric gradients in January.

[32] The interactions between vertical and latitudinal gradients in CH₄ (also valid for tracers in the troposphere with lifetimes greater than the interhemispheric transport time of about 1.3 years; see Figure S5 for SF₆ results) are schematically depicted in Figure 9b. Based on our analysis, we hypothesize that (1) vertical transport is driven by the strength of convection as well as turbulent mixing in the boundary layer (BL) and (2) meridional gradients depend mainly on the mixing in the BL for sites close to emissions and on the horizontal advection scheme for the remote/background sites. However, there is interaction between the turbulent mixing, convection, and advection processes in the model. A study using ACTM [Patra *et al.*, 2009b] suggested that the turbulent mixing transports emission signals to the 900–800 mb height layer, and the convective processes transport species from the BL to the middle and upper troposphere (MUT). Most of the interhemispheric transport due to advection occurs at higher altitudes. Thus, a model transport with weaker turbulent mixing and

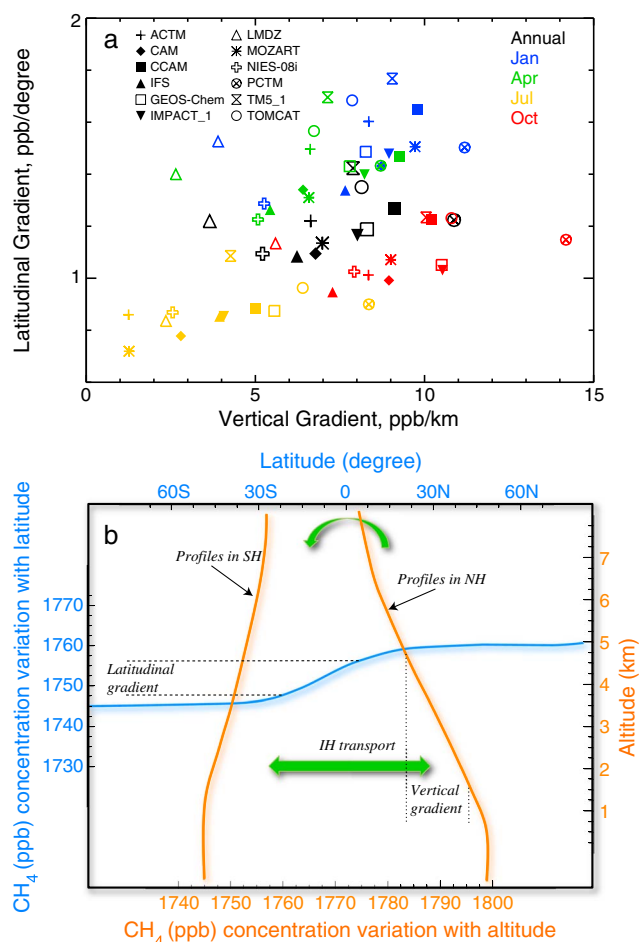


Figure 9. (a) Modeled vertical gradients in the NH between 900 hPa (~1 km) and 500 hPa (~5 km) in the latitude range of 30°N–50°N are plotted versus the modeled latitudinal gradients between the NH (30°N–50°N) and the SH (50°S–30°S), averaged over the height range of 900–500 hPa (~1.0–5.5 km). Results are shown for different months, representing boreal winter, spring, summer, and autumn (January, April, July, and October, respectively) and for annual mean. (b) A schematic of the relationship between the vertical and interhemispheric transports is depicted in the lower panel.

convection has a tendency toward steeper meridional gradient in the simulated concentrations at lower altitudes but not at higher altitudes (6–8 km).

[33] As discussed in *Patra et al.* [2011a] and shown in Figure 9a, the TM5 model produces one of the largest latitudinal gradients in CH₄ among all the models that participated in the TransCom-CH₄ experiment. However, we find in this study that the NH vertical gradients simulated by TM5 are not the largest. The latitudinal gradients shown in Figure 6 suggest that the stronger gradients in the TM5 simulations are mainly due to low SH concentrations compared to other models, likely to be caused by slower meridional transport. PCTM produced the largest vertical gradients below 1–2 km (refer to Figures 3 and 9a), most likely due to trapping of emissions within the planetary boundary layer. However, the simulated interhemispheric gradients are not extreme because stronger vertical

gradients for PCTM in both the hemispheres (Figure 5c) result in an interhemispheric gradient that is close to the multimodel average. All other models suggest that a stronger vertical gradient in NH troposphere corresponds to a stronger interhemispheric gradient in CH₄ concentrations.

4. Conclusions

[34] We assessed zonal, meridional, and vertical transports of tropospheric CH₄ using the chemical transport models (CTMs) and two emission scenarios (CTL and EXTRA) in comparison with aircraft measurements. The model-model difference is large near the surface in source regions and during strong convection and small in the middle/upper troposphere and over the marine background regions. The model-observation differences are controlled predominantly by the model transport and the surface emission rather than the loss rates of CH₄. At most sites, the simulated concentrations vary around the observed values, while at three sites, the model results are systematically biased relative to the observed value. The positive (at Surgut, Russia) and negative (at South Great Plain, United States, and Santarem, Brazil) biases, systematic for most models, can be attributed to higher and lower CH₄ emissions as estimated in the CTL case. These model-observation comparison results are generally consistent for simulations using both the emission scenarios, CTL or EXTRA (except for Surgut, where simulations using lower emissions over the Siberian region, as in EXTRA, showed better model-observation agreements).

[35] Observed CH₄ profiles show near-zero vertical gradients above 3 km, where models indicate that the convective activity is the primary driver of mixing (all seasons over the Amazon and summer months in the higher latitudes), and elevated concentrations in the upper troposphere region, when measurements are available over Surgut. In contrast, stronger decreases with altitudes above 3 km are observed in the middle- and high-latitude land regions, where the anthropogenic emissions are intense (e.g., TGC, HFM, and SUR) compared to the lower emissions over the background marine sites (e.g., HAA and ULB). The model-model differences are found to be greatest at sites located over intense emission regions for the height below 3 km. In the middle and upper troposphere (MUT), greater model-model differences are found over the regions with stronger convective activities (e.g., SAN and NH sites during summer). These two results suggest that the turbulent mixing (acting below 3 km) and deep cumulus convection (acting in the MUT region) parameterizations in the CTMs are less similar compared to the other transport processes, such as advection (except for one model).

[36] Interhemispheric gradients of the simulations and observations were 1.5 ± 0.1 and 1.3 ± 0.2 ppb/deg for the lower and middle troposphere, respectively. In an effort to understand the origin of model-model differences in interhemispheric gradients, we have shown scatterplots of vertical gradients in CH₄ concentrations between lower and middle troposphere and latitudinal gradients between the two hemispheres. Generally, the models that produced higher vertical gradients for CH₄ (and also SF₆) concentrations also produced steeper interhemispheric gradients near the surface. In models with underestimated vertical mixing mainly due to boundary-layer turbulent mixing and parameterized

convection, tracers tend to get trapped near the sources in the lower troposphere. In this case, the model is likely to overestimate meridional gradients in tracer concentrations, resulting from relative inefficient advective transport between the hemispheres (except for two exceptions in PCTM and TM5).

[37] **Acknowledgments.** This work was supported by JSPS/MEXT KAKENHI-A (grant 22241008). A. Fraser was supported by the UK Natural Environment Research Council National Centre for Earth Observation. We acknowledge the work of J. McGregor and M. Thatcher in the development of CCAM. CCAM simulations were undertaken as part of the Australian Climate Change Science Program and used the NCI National Facility in Canberra, ACT, Australia. R. Prinn and M. Rigby were supported by NASA-AGAGE grants NNX07AE89G and NNX11AF17G to MIT. M. Rigby was also supported by a NERC Advanced Fellowship. The TOMCAT work at the University of Leeds was supported by NERC/NCEO. The research leading to the IFS results has received funding from the European Community's Seventh Framework Programme [FP7 THEME (SPA.2011.1.5-02)] under grant 283576 in the context of the MACC-II project (Monitoring Atmospheric Composition and Climate—Interim Implementation). We sincerely thank all three anonymous reviewers for critical evaluation and providing very helpful comments and suggestions for improving the article.

References

- Beck, V., et al. (2012), Methane airborne measurements and comparison to global models during BARCA, *J. Geophys. Res.*, *117*, D15310, doi:10.1029/2011JD017345.
- Belikov, D., S. Maksyutov, T. Miyasaka, T. Saeki, R. Zhuravlev, and B. Kiryushov (2011), Mass-conserving tracer transport modelling on a reduced latitude-longitude grid with NIES-TM, *Geosci. Model Dev.*, *4*, 207–222, doi:10.5194/gmd-4-207-2011.
- Bergamaschi, P., et al. (2009), Inverse modeling of global and regional CH₄ emissions using SCIAMACHY satellite retrievals, *J. Geophys. Res.*, *114*, D22301, doi:10.1029/2009JD012287.
- Bian, H., S. R. Kawa, M. Chin, S. Pawson, Z. Zhu, P. Rasch, and L. Wu (2006), A test of the representation of convective cloud transport in a model of CO₂ transport, *Tellus*, *58B*(5), 463–475, doi:10.1111/j.1600-0889.2006.00212.X.
- Corbin, K. D., and R. M. Law (2011), Extending atmospheric CO₂ and tracer capabilities in ACCESS, CAWCR Tech. Rep. 35, The Centre for Australian Weather and Climate Research, ISBN:978-1-921826-177, Aspendale.
- Denning, A. S., et al. (1999), Three-dimensional transport and concentration of SF₆: A model intercomparison study (TransCom-2), *Tellus*, *51B*, 266–297, 1999.
- Dlugokencky, E. J., R. C. Myers, P. M. Lang, K. A. Masarie, A. M. Croswell, K. W. Thoning, B. D. Hall, J. W. Elkins, and L. P. Steele (2005), Conversion of NOAA atmospheric dry air CH₄ mole fractions to a gravimetrically prepared standard scale, *J. Geophys. Res.*, *110*, D18306, doi:10.1029/2005JD006035.
- Chipperfield, M. P. (2006), New version of the TOMCAT/SLIMCAT off-line chemical transport model: Intercomparison of stratospheric tracer experiments, *Q. J. R. Meteorol. Soc.*, *132*, 1179–1203, doi:10.1256/qj.05.51.
- Emmons, L. K., et al. (2010), Description and evaluation of the Model for Ozone and Related chemical Tracers, version 4 (MOZART-4), *Geosci. Model Dev.*, *3*, 43–67, doi:10.5194/gmd-3-43-2010.
- Fraser, A., C. Chan Miller, P. I. Palmer, N. M. Deutscher, N. B. Jones, and D. W. T. Griffith (2011), The Australian methane budget: interpreting surface and train-borne measurements using a chemistry transport model, *J. Geophys. Res.*, *116*, D20306, doi:10.1029/2011JD015964.
- Fung, I., J. John, J. Lerner, E. Matthews, M. Prather, L. P. Steele, and P. Fraser (1991), Three-dimensional model synthesis of the global methane cycle, *J. Geophys. Res.*, *96*(D7), 13,033–13,065.
- Gatti, L. V., J. B. Miller, M. T. S. D'Amelio, A. Martinewski, L. S. Basso, M. E. Gloor, S. Wofsy, and P. Pans (2010), Vertical profiles of CO₂ above eastern Amazonia suggest a net carbon flux to the atmosphere and balanced biosphere between 2000 and 2009, *Tellus*, *62B*, 581–594, doi:10.1111/j.1600-0889.2010.00484.X.
- Gent, P. R., S. G. Yeager, R. B. Neale, S. Levis, and D. A. Bailey (2009), Improvements in a half degree atmosphere/land version of the CCSM, *Clim. Dyn.*, *79*, 25–58, doi:10.1007/s00382-009-0614-8.
- Graedel, T. E., and P. J. Crutzen (1993), *Atmospheric change: An Earth system perspective*, pp. 446, Freeman, New York, ISBN:0716723344.
- Hourdin, F., et al. (2006), The LMDZ4 general circulation model: climate performance and sensitivity to parameterized physics with emphasis on tropical convection, *Clim. Dyn.*, *27*, 787–813, doi:10.1007/s00382-006-0158-0.
- Ito, A., and M. Inatomi (2012), Use and uncertainty evaluation of a process-based model for assessing the methane budget of global terrestrial ecosystems, *Biogeosciences*, *9*, 759–773, doi:10.5194/bg-9-759-2012.
- Kawa, S. R., D. J. Erickson III, S. Pawson, and Z. Zhu (2004), Global CO₂ transport simulations using meteorological data from the NASA data assimilation system, *J. Geophys. Res.*, *109*, D18312, doi:10.1029/2004JD004554.
- Krol, M. C., S. Houweling, B. Bregman, M. van den Broek, A. Segers, P. vanVelthoven, W. Peters, F. J. Dentener, and P. Bergamaschi (2005), The two-way nested global chemistry-transport zoom model TM5: Algorithm and applications, *Atmos. Chem. Phys.*, *5*, 417–432, doi:10.5194/acp-5-417-2005.
- Law, R. M., E. A. Kowalczyk, and Y.-P. Wang (2006), Using atmospheric CO₂ data to assess a simplified carbon-climate simulation for the 20th century, *Tellus, Ser. B*, *53*, 427–437, doi:10.1111/j.1600-0889.2006.00198.X.
- Law, R. M., et al. (2008), TransCom model simulations of hourly atmospheric CO₂: Experimental overview and diurnal cycle results for 2002, *Global Biogeochem. Cycles*, *22*, GB3009, doi:10.1029/2007GB003050.
- Machida, T., et al. (2001), Temporal and spatial variations of atmospheric CO₂ mixing ratio over Siberia, paper presented at the Sixth International CO₂ Conference, Sendai, Japan.
- Miyazaki, K., P. K. Patra, M. Takigawa, T. Iwasaki, and T. Nakazawa (2008), Global-scale transport of carbon dioxide in the troposphere, *J. Geophys. Res.*, *113*, D15301, doi:10.1029/2007JD009557.
- Nakazawa, T., K. Miyashita, S. Aoki, and M. Tanaka (1991), Temporal and spatial variations of upper tropospheric and lower stratospheric carbon dioxide, *Tellus, Ser. B*, *43*, 106–117.
- Olivier, J. G. J., and J. J. M. Berdowski (2001), Global emissions sources and sinks, in *The Climate System*, edited by J. Berdowski, R. Guicherit, and B. J. Heij, pp. 33–78, A. A. Balkema Publishers/Swets & Zeitlinger Pub., Lisse, Netherlands, ISBN:9058092550.
- Patra, P. K., et al. (2009a), Growth rate, seasonal, synoptic, diurnal variations and budget of methane in lower atmosphere, *J. Meteorol. Soc. Jpn.*, *87*(4), 635–663, doi:10.2151/jmsj.87.635.
- Patra, P. K., M. Takigawa, G. S. Dutton, K. Uhse, K. Ishijima, B. R. Lintner, K. Miyazaki, and J. W. Elkins (2009b), Transport mechanisms for synoptic, seasonal and interannual SF₆ variations and “age” of air in the troposphere, *Atmos. Chem. Phys.*, *9*, 1209–1225, doi:10.5194/acp-9-1209-2009.
- Patra, P. K., et al. (2011a), TransCom model simulations of CH₄ and related species: Linking transport, surface flux and chemical loss with CH₄ variability in the troposphere and lower stratosphere, *Atmos. Chem. Phys.*, *11*, 12,813–12,837, doi:10.5194/acp-11-12813-2011.
- Patra, P. K., Y. Niwa, T. J. Schuck, C. A. M. Brenninkmeijer, T. Machida, H. Matsueda, and Y. Sawa (2011b), Carbon balance of South Asia constrained by passenger aircraft CO₂ measurements, *Atmos. Chem. Phys.*, *11*, 4163–4175, doi:10.5194/acp-11-4163-2011.
- Rottman, D. A., et al. (2004), IMPACT, the LLNL 3-D global atmospheric chemical transport model for the combined troposphere and stratosphere: Model description and analysis of ozone and other trace gases, *J. Geophys. Res.*, *109*, D04303, doi:10.1029/2002JD003155.
- Sawa, Y., T. Machida, and H. Matsueda (2012), Aircraft observation of the seasonal variation in the transport of CO₂ in the upper atmosphere, *J. Geophys. Res.*, *117*, D05305, doi:10.1029/2011JD016933.
- Spivakovsky, C., et al. (2000), Three-dimensional climatological distribution of tropospheric OH: Update and evaluation, *J. Geophys. Res.*, *105*(D7), 8931–8980.
- Stephens, B. B., et al. (2007), Weak northern and strong tropical land carbon uptake from vertical profiles of atmospheric CO₂, *Science*, *316*(5832), 1732–1735, doi:10.1126/science.1137004.
- Tans, P. P., et al. (1996), *Carbon Cycle (Group Report), Climate Monitoring and Diagnostics Laboratory, No. 23, Summary Report 1994–1995*, edited by D. J. Hoffman, J. T. Peterson, and R. M. Rosson, <http://www.esrl.noaa.gov/gmd/publications/annrpt23/contents.html>, U.S. Department of Commerce, Boulder, Colo.
- van der Werf, G. R., J. T. Randerson, L. Giglio, G. J. Collatz, P. S. Kasibhatla, and A. F. Arellano Jr. (2006), Interannual variability in global biomass burning emissions from 1997 to 2004, *Atmos. Chem. Phys.*, *6*, 3423–3441, doi:10.5194/acp-6-3423-2006.
- Xiong, X., C. D. Barnett, Q. Zhuang, T. Machida, C. Sweeney, and P. K. Patra (2010), Mid-upper tropospheric methane in the high Northern Hemisphere: Spaceborne observations by AIRS, aircraft measurements, and model simulations, *J. Geophys. Res.*, *115*, D19309, doi:10.1029/2009JD013796.
- Zhou, L. X., D. Kitzis, and P. P. Tans (2009), Report of the fourth WMO round-robin reference gas intercomparison, 2002–2007, in *Report of the 14th WMO meeting of Experts on Carbon Dioxide Concentration and Related Tracer Measurement Techniques*, edited by T. Laurila, pp. 40–43, Helsinki, Finland, September 10–13, 2007, WMO/GAWReport No. 186.